Dynamic Wave Propagation in a Single Lap Joint

Paper reports on the results of a two-dimensional dynamic photoelastic study of the stresses in a short single lap joint when an elastic impulse wave traverses it from one plate into the other

by L.W. Zachary and C.P. Burger

ABSTRACT—Dynamic photoelasticity was used to study the stresses when an impulse wave propagates through a single lap joint. An explosive was detonated in one of the adherends. The resulting stress wave propagated down the adherend and through the joint area. At the junction between the adherends, the stress wave interacted with the ends of the adherends and significant changes in the stress wave occurred. The stress wave then propagated through the joint and, in doing so, interacted with the two square corners at the adhesive/adherend interface. It was found that a significant biaxial tensile stress occurs at one of the corners.

With only the usual black and white photographs, the ordering and interpretation of the photoelastic-fringe orders was difficult. The paper indicates how color photographs were used to simplify identification of the fringes.

Introduction

Much has been written about the static analysis of adhesive lap joints. Relevant works are summarized in Refs. 1 through 3. The literature on dynamic and impulsive stresses in such joints, however, is almost nonexistent. Yet, such loads are often more important to the fatigue and fracture resistance of lap joints than the static condition. This paper reports on the results of a two-dimensional dynamic photoelastic study of the stresses in a short single lap joint when an elastic impulse wave traverses it from one plate into the other.

Technique

The photoelastic model consisted of two $1 \times \frac{1}{4} \times 8\frac{1}{2}$-in. ($25 \times 6 \times 212$-mm) strips of CR-39 glued together as shown in Fig. 1. The adhesive was a fast-curing epoxy which permitted the wave to be transmitted through the joint with no noticeable reflections. The residual curing stresses at the interface were controlled to a level that was undetectable in terms of observable initial birefringence.

The impulsive wave was created by exploding a 100-mg charge of lead azide at the end of the lower plate of Fig. 1. In order to generate an approximately plane wave, the charge was loaded into a separate cap of CR-39. A small transverse hole was drilled through the cap, threaded with a thin 'exploding' wire, and then filled with the explosive. The cap was then glued onto the end of the model with Eastman 910 cement. The explosive was detonated by exploding the wire with a 2000-V pulse. The time of the pulse was taken as 'time zero'. The glue line between the cap and the model was made to be weak in tension. It permitted the compressive part of the impulse wave to enter the model, but it fractured soon after the tensile or unloading tail of the wave began to develop. The resultant wave in the model was a long flat compressive wave with virtually no tensile component.

The dynamic photoelastic data were obtained with a Cranz-Schardin-type spark camera as described by Ligon.[4] It provided 16 dynamic frames of the photoelastic patterns at preselected times during an event. The data were recorded as isochromatic fringes at equivalent exposure times of about 0.6 μs/frame. Monochromatic light was obtained by placing a set of Kodak Wratten filters (No. 34A) immediately behind the lenses. The fringe resolution under these conditions was better than 20 fringes/in. as reported by Burger and Riley.[5] While the resolution is good, the interpretation of the fringe patterns obtained in this manner is difficult at the best of times and becomes almost formidable in complicated stress fields such as occurred in the lap joint reported here.

Photoelastic-fringe patterns recorded in white light are easier to interpret since the direction of increase or decrease in fringe orders as well as points of zero fringe order are easily identified. The resolution at higher fringe order are, however, poorer than with monochromatic light and the fringe orders must be calibrated by matching their colors to the monochromatic-fringe orders. For consistent color rendering, the exposure and processing of the color film must be closely controlled.

The arc sources provided a reasonably full color spectrum but suffered from inherent variations in light intensity from one arc to another. Since the effective apertures of the lenses could not be varied, the only way in which the individual exposures on the color film could be controlled was by placing different neutral density filters behind each lense (in place of the violet filters) and adjusting the density of each individual lens until all 16 negatives had the same illumination. The resulting color slides of the dynamic event were consistent and of good quality.

L.W. Zachary (SESA Member) and C.P. Burger (SESA Member) are Assistant Professor and Professor, respectively, Department of Engineering Science and Mechanics, Iowa State University, Ames, IA 50011.

Paper was presented at 1978 SESA Spring Meeting held in Wichita, KS on May 14-19.

Original manuscript submitted: November 20, 1979. Final version received: January 22, 1980.

Two methods were used to calibrate the colored patterns with respect to monochromatic black and white fringes: a beam in pure bending and a disk in diametrical compression. Stress-frozen calibration models were mounted in the camera in place of the dynamic model and the camera was fired in exactly the same way as during a regular test. The film pack of the camera was loaded with a color film for four lenses, and black and white film for the others. The lenses recording color pictures had the necessary correction filters in, while the remainder were filtered with the regular Wratten 34A filters. The successive color tones were calibrated against the monochromatic black and white fringes. Good calibration was possible up to the eighth-order isochromatic. Higher-order fringes could be identified, but their precise location was not well established.

Figure 2 is an example of a monochromatic-fringe pattern at about 150 μs.

Results

The dynamic photoelastic method provided 16 consecutive slides of the isochromatic fringes in the model. Six of these slides were used to obtain the data presented in Fig. 3. All times are given in microseconds after detonating the explosive. The dilatational (P-wave) velocity was 42,000 in./s (1070 m/s). This means that the dilatational wave progressed approximately 1 in. in 14 μs. This value can be used to visualize the progression of the different waves through the model.

The thin dashed lines in the first two frames of Fig. 3 (115 μs and 125 μs) show the theoretical positions of the dominant wave fronts that should be present at these times. At 115 μs, the wave motion is still almost wholly in the first plate (lower adherend). The compressive dilatation wave (P-wave) is just past the first corner of the joint. The wave front is straight (a plane wave) in the lower adherend. The corner is a source that generates P and S waves with their associated PS head wave. These waves have separated and are more readily identified in the next frame (125 μs). The P-wave in the lower adherend travels at grazing incidence to the free surface. It generates a reflected PS wave which travels away from the point of reflection at the shear velocity. For CR-39, this wave is set at an angle of 35 deg with the surface. Where it intersects the second free surface, it generates another dilitational wave (PSP) and a shear wave (PSS). The PSP wave is perpendicular to the free surface and the PSS wave is reflected at 35 deg to the surface. References 5-8 explain the occurrence of these waves.

The frame at 125 μs shows one additional detail: when the first reflected shear wave (PS) from the top surface reached the corner at the joint line (i.e., when P first reached that position) the reflection ceased and the wave propagated outward at shear velocity as if the corner was a source. This is shown as a circular S wave tangent to the straight portion of the PS wave.

In the next three frames (131, 145 and 156 μs), only the fronts of the original P-wave are shown. When the compressive dilitation wave reaches the vertical face CD at the end of the lower adherend, it is reflected as a plane tensile dilitational wave (PP) (131 μs). This tensile stress subtracts from the remaining portion of the compressive wave that is still moving towards the edge. The portion of the energy in the original P-wave that passed through the joint into the second plate (upper adherend) continues to propagate down that plate as if it had its source at the first corner of the joint. When it first reaches the top edge of the plate in the top right-hand corner it starts to reflect from that edge as a tensile (PP) wave. None of the remaining secondary waves is shown in these three frames.

On the free surfaces of the model, the photoelastic-fringe orders represent scaled values of the tangential surface stresses. The stresses normal to the surfaces are zero. These stresses are shown on all horizontal and vertical surfaces in Fig. 3. The horizontal stresses are plotted as solid lines with compression above the line and tension below the line. Stresses on the two vertical surfaces

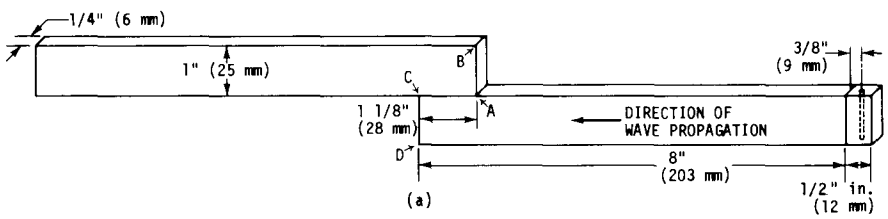

Fig. 1—Photoelastic model

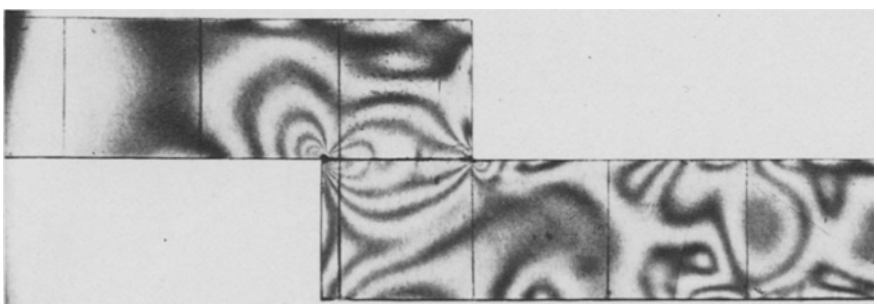

Fig. 2—Dynamic photoelastic pattern

are drawn as point-dotted lines with compression to the right of the line and tension to the left.

The symmetry of the photoelastic data for the incident P-wave is clearly shown in the first frame (115 μs). The shape of the wave as evidenced by the surface stresses on both the upper and the lower surfaces of the plate is almost identical. It reaches a plateau about 1 in. (25 mm) behind its front. The plateau extends for about 0.75 in. (18 mm) and then dips as the reflected PS-wave from the opposite surface comes into the field. The overall length of the compression front of this wave is just short of 3 in. (76 mm). The solid lines, therefore, represent the spatial position and shape of the surface stresses caused by the elastic waves. The fronts of these stress waves coincide with the positions where the wave fronts predict that they should be.

The plateau level on the upper free surface at 115 μs was chosen as the reference stress (σ_n) for a dynamic stress-concentration factor K_d. The eighth-order fringe corresponded to this value. Thus, at any point on a free surface

$$K_d = \frac{|\sigma|}{|\sigma_n|} = \frac{N}{N_n}$$

where the subscript n denotes the reference condition at 115 μs and N = fringe order on the boundary.

From the frame at 125 μs it is seen that the dip in the P-wave amplitude only reduces K_d to 0.6 before it again rises to $K_d = 1$.

At 115 μs, the P-wave has just entered the joint area and a very slight surface stress should be evident in the corner on the vertical face AB. This beginning of the observable optical response does not, however, coincide with the projected position of the P-wave along that face. It even lags behind the S-wave.

Ten microseconds later, at 125 μs, the front of the P-wave should be approaching two reflective surfaces: the left-end CD of the lower adherend and the top surface of the upper adherend. The optical data in the lower adherend support this prediction; the fringes in the upper adherend (face AB) do not. The apparent wave front as evidenced from the fringe data is circular over an arc of only 80 deg. The apparent 'source' of this circular arc is not the corner A, but a point slightly below and to the left of the corner. This point is marked as a black circle on the frames for 125 and 131 μs. The exact behavior of a stress wave as it rounds a sharp corner is not known. Neither analytic nor experimental data are available. It is reasonable

Fig. 3—Dynamic stress distributions in a lap joint

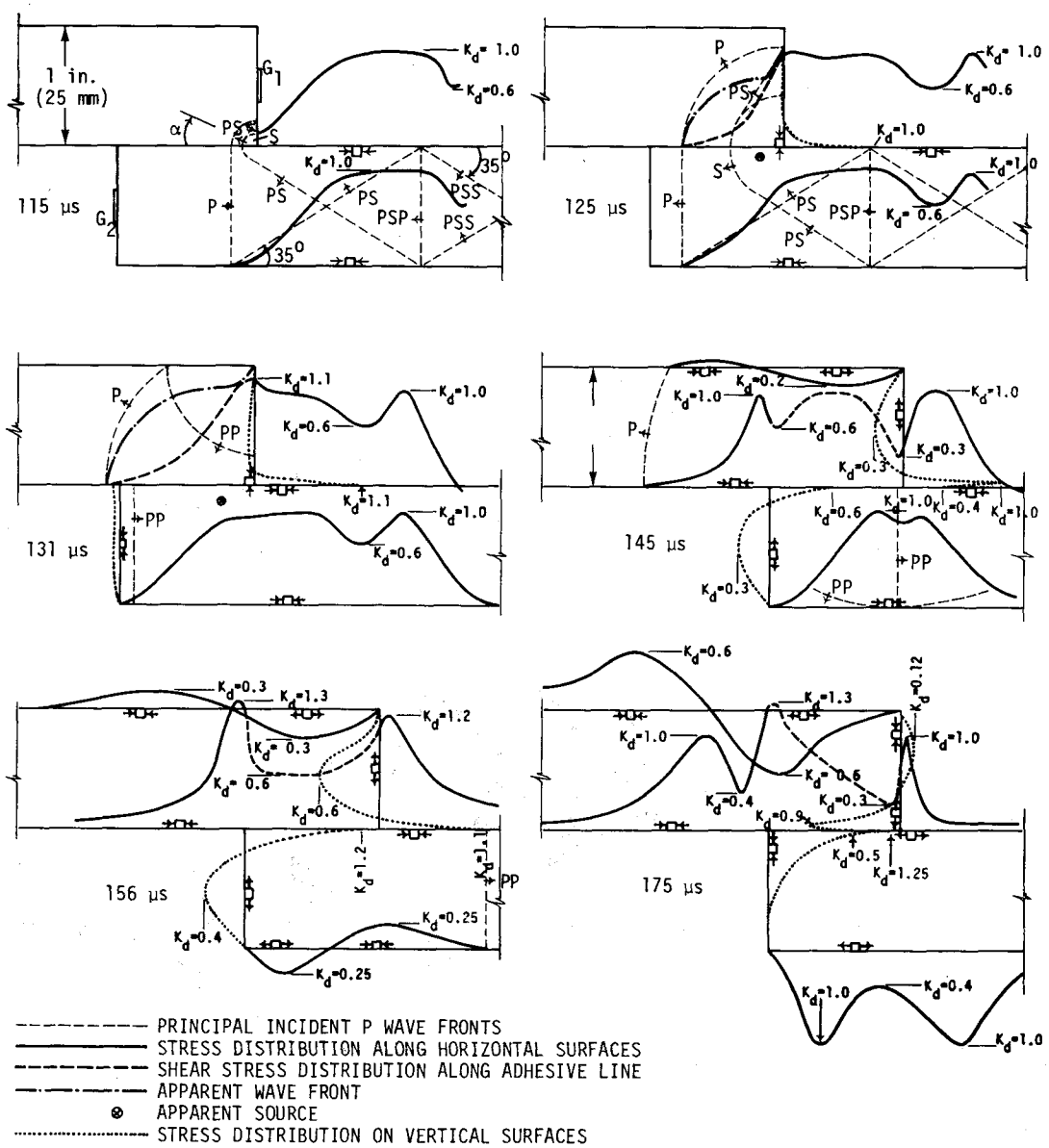

to argue, however, that the specific energy in the wave should decrease with the angle α (see 115 μs) and may be very small as α approaches 90 deg. Since a finite threshold value of $(\sigma_1 - \sigma_2)$ is necessary before the film records an image, the weaker wave front will cause the first change of color to appear later in the wave. For very weak waves the optical threshold does not coincide with the wave front.

At 125 μs, the magnitude of the surface stress on the vertical face is a small tension everywhere except near the corner, where it changes sign and rises very rapidly to a compressive stress with $K_d = 1$. In all subsequent frames, the surface stresses in the corner have the same magnitude on the vertical face as on the horizontal face. They also have the same sign. An element at the corner is, therefore, under an equal biaxial state of stress in the plane of the model.

When the state of stress on the first vertical face AB and specifically the stresses near the corner is traced through all six frames, information is revealed which is important with respect to initiation of fracture at point A. The dynamic response of the face is such that a significantly large tension develops over most of the face while leaving the corner in compression until sometime between 156 and 175 μs when the signs reverse rapidly to yield a biaxial tension of $K_d = 0.9$ at the corner.

The signs of the stresses on the face were confirmed with a strain gage as discussed later. The state of stress is due to a flexural wave which develops as the wave front encounters the corner. Such flexural waves have been observed by Crowley, Phillips and Taylor[8] for a pulse that propagates around a sharp 90-deg corner in a beam of uniform 'depth'. Its growth can be explained by a displacement argument as follows.

A rectangular element at corner A in the lower adherend is displaced to the left by the incident compression pulse. This will cause a displacement wave to move up the vertical face towards the top corner. The displacement of the original element, however, is likely to be irrotational, or nearly so. Since the envelope of the particle displacements along face AB has to be tangent to the vertical free surface ahead of the flexure wave, a double curvature is necessary to satisfy the two end conditions. A negative curvature arises near the corner which causes compressions on the free surface. A positive curvature, which causes tensile stresses, appears over the rest of the face and moves up the face until the wave front reaches the top corner. Stress reversal occurs at the inflexion point of the flexural wave.

The corner A will undergo an 'unloading' after the original P-wave has passed. This occurs at about the time of the last frame (175 μs). The actual reversal in sign to a tensile stress is particularly rapid because the reflected PP-wave from end CD of the lower adherend reaches point A at the same time and wipes out the remainder of the original P-wave. This forces a displacement in the reverse direction of the corner element's original displacement and, thus, produces the tensile stress at the corner.

A similar argument explains the states of stress along the second vertical face. The wave incident on the free surface CD causes outward particle displacements. The whole face, however, cannot be displaced equally because of its attachment to the upper adherend. Particle displacements immediately above the joint are less than on the free face below the joint. In addition to this effect, the displacements above the joint in the upper adherend reduce rapidly when going from the lower surface to the top surface because the intensity of the impulsive wave diminishes in this direction. A clockwise rotation of an element immediately above the joint is likely because of this diminishing displacement field. This will cause a flexure wave which is initially all tension on the vertical face. As the outward displacements on the vertical free face build and the rotation of the upper element decreases, a double-curvature flexure wave develops, yielding compression in the corner and tension further down the face. The reflected PP and shear waves finally interact to produce a continuous compression along the free face. The photoelastic data show these effects, and the signs of the surface stresses were confirmed with a strain gage.

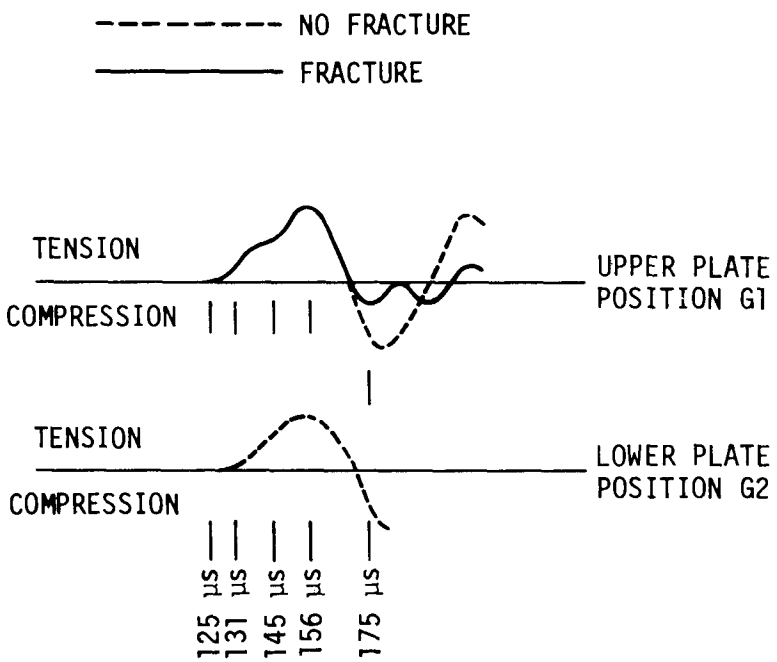

Fig. 4—Strain-gage data on midpoint of vertical sides

This essentially concludes the stress effects caused by the passage of the primary P-wave through the joint. If the joint separates, it is likely to do so from the right-hand corner. For the sake of clarity, the surface waves on all the horizontal edges are included in Fig. 3.

Figure 4 shows the strain vs. time record obtained from two strain gages mounted at positions G_1 and G_2, Fig. 3 (115 μs). Although these records were taken primarily to confirm the presence of tensions on the two faces, they correlate very well with the overall description of the stress history. The solid line was obtained during a test when only gage G_1 was recording. The joint separated under the impulse. The dotted lines were obtained from strain gages G_1 and G_2 in a case when the joint did not separate. The initial waves were identical in the two cases. For position G_1, the two curves coincide on the tension side. They start to deviate from each other at around 170 μs, which is almost exactly when the peak tension in the corner would have occurred (Fig. 3, 175 μs). When the joint separated, the energy in the upper plate was isolated from its main source, which is the incident P-wave in the lower plate. The compression at G_1 does not build up to the same level as when the joint remains intact. The corner on the top plate is now free and starts to unload as shown by the compressive oscillations of the solid line. The record for the gage at position G_2 was lost because the lead-wire tabs separated from the plate, possibly under the influence of a large reflected tension normal to the glue line of the tab. The ratios of the stresses recorded at the relevant time intervals agree completely with those obtained from the photoelasticity data for positions G_1 and G_2.

At internal points in the model, the fringe orders are proportional to the maximum in-plane shear stresses. For some symmetrical waves, the in-plane principal stresses can be separated without using isoclinic data.[5,6] This was not done here. The fringe order along the joint is, however, shown in Fig. 3 as the chain-dotted line which extends from the right-hand vertical face AB to the opposite left face CD. This portion of the wave, although continuous with respect to the edge stresses, should not be interpreted in the same way as the edge stresses. It contains only information about the maximum in-plane shear stress and does not in itself indicate the shape of the wave. At 145 μs, $K_d = 1$ is obtained and should be interpreted as being equal to the maximum shear stress occurring at the plateau of the P-wave (115 μs). This represents the largest in-plane shear stress recorded along internal regions of the joints.

The waves that are finally established on the upper and lower faces of the upper adherend are worth some study. The wave on the lower face remains completely compressive (145 to 175 μs) during the time interval observed here. It does not resemble the original P-wave in shape because it has been modified by several secondary dilatation and shear waves. Its peak compressive value of $K_d = 1.3$ (156 μs) is 30 percent higher than anything recorded in the undistrubed initial P-wave (lower adherend, lower surface prior to time 131 μs). The shape and intensity of this wave changes across the upper adherend. At the top surface, the effects of the upper free corner acts to change the shape of the wave. The records for the surface wave along the top edge show the development and steadily increasing tensile component. This reaches a maximum value of $K_d = 0.6$ at 175 μs, despite the observation that the original P-wave (125 and 145 μs) displayed only a very small tensile tail. The presence of this new tension has significance if other structural discontinuities should occur along or near the top surface of the second plate. The peaks of this wave do not travel at the P-wave velocity. They progress at between 25 and 28 μs/in. (1-1.1 μs/in., 35700-40000 in./s, 907-1020 m/s), i.e., only slightly slower than pure-shear waves.

Conclusion

The ratios of joint length, adherend thickness and wavelength used in this study were, admittedly, severe. It is, nevertheless, important to recognize that, under impulse loading, severe tensile and shear stresses can develop in a joint such as this. These stresses are rendered more significant because at the strain rates involved, all known adhesives behave in a hard, brittle fashion.[9] Under these conditions, the consequences of localized stress concentrations can be particularly serious, especially when the dynamic stresses are superimposed onto localized shrinkage stresses and the quasi-static loads for which the joint was initially designed. If an impulse occurs when the joint is below the glass-transition temperature, its effects are even more dangerous.[10]

In a wide joint, the development of triaxial states of stress generally occurs in joints. If the joint is thin, the triaxiality can be severe. This paper suggests that these stresses may be large triaxial tensions at the first corner of the joint. Such a condition is particularly favorable to brittle fracture.[11]

Acknowledgments

The research presented here was conducted with funds provided by the Engineering Research Institute and the Department of Engineering Science and Mechanics at Iowa State University. Much of the experimental data were collected by David van Haaften who was an undergraduate assistant at the time and is now with E.G. & G., Idaho Falls, ID.

References

1. *Murphy, M.M. and Lenoe, E.M., "Stress Analysis of Structural Joints and Interfaces—A Selected Annotated Bibliography," Army Materials and Mechanics Research Center, Watertown, MA, AMMRC MS 74-10 (1974).*

2. *Zachary, L.W. and Rogge, T.R., "Stresses in Adhesive Layers with Cracks and Inclusions," Ninth SECTAM, May 4-5, Nashville, TN (1978).*

3. *Anderson, G.P., Bennett, S.J. and DeVries, K.L., Analysis and Testing of Adhesive Bonds, Academic Press, New York (1977).*

4. *Ligon, J.B. and Riley, W.F., "Close-field Optical Analysis of an Explosive-loading Function,"* EXPERIMENTAL MECHANICS, **14** *(5), 184-189 (1974).*

5. *Burger, C.P. and Riley, W.F., "Effects of Impedance Mismatch on the Strength of Waves in Layered Solids,"* EXPERIMENTAL MECHANICS, **14** *(3), 129-137 (1974).*

6. *Riley, W.F. and Dally, J.W., "Photoelastic Analysis of Stress Wave Propagation in a Layered Model," Geophysics* **31** *(5), 881-889 (1966).*

7. *Cagniard, L., Flinn, E.A. and Dix, C.H., Reflection and Refraction of Progressive Seismic Waves, Mc-Graw Hill, New York (1962).*

8. *Achenbach, J.D., Wave Propagation in Elastic Solids, North-Holland Publishing Co., Amsterdam (1973).*

9. *Crowley, F.B., Phillips, J.W. and Taylor, C.E., "Pulse Propagation in Straight and Curved Beams—Theory and Experiment," J. of Appl. Mech.,* **41** *(1), 71-76 (1974).*

10. *Turner, A., "Role of Bulk Properties of Adhesives," in Treatise on Adhesion and Adhesives (ed. R.L. Patric), Marcel Dekker, New York (1967).*

11. *Kaeble, D.H., "Rheology of Polymers Used as Adhesives," Treatise on Adhesion and Adhesives (ed. R.L. Patric), Marcel Dekker, New York (1967).*

12. *Irwin, G.R., "Fracture Mechanics Applied to Adhesive Systems," in Treatise on Adhesion and Adhesives (ed. R.L. Patric), Marcel Dekker, New York (1967).*